

Persistence of two-dimensional topological insulator state in wide HgTe quantum well

E. B. Olshanetsky,¹ Z. D. Kvon,^{1,2} G. M. Gusev,³ A. D. Levin,³

O. E. Raichev,⁴ N. N. Mikhailov,¹ and S. A. Dvoretzky,¹

¹*Institute of Semiconductor Physics, Novosibirsk 630090, Russia*

²*Novosibirsk State University, Novosibirsk 630090, Russia*

³*Instituto de Física da Universidade de São Paulo, 135960-170, São Paulo, SP, Brazil and*

⁴*Institute of Semiconductor Physics, NAS of Ukraine, Prospekt Nauki 41, 03028 Kyiv, Ukraine*

(Dated: August 23, 2018)

Our experimental studies of electron transport in wide (14 nm) HgTe quantum wells confirm persistence of a two-dimensional topological insulator state reported previously for narrower wells, where it was justified theoretically. Comparison of local and nonlocal resistance measurements indicate edge state transport in the samples of about 1 mm size at temperatures below 1 K. Temperature dependence of the resistances suggests an insulating gap of the order of a few meV. In samples with sizes smaller than 10 μm a quasiballistic transport via the edge states is observed.

The topological insulators (TI) represent a quantum state of condensed matter with insulating bulk and conducting gapless states at the surface or edge [1–4]. The existence of such materials is justified within a concept of topological ordering introducing order parameters which are often expressed as invariant integrals over the momentum space. In the presence of time reversal symmetry, the materials with energy band gaps (band insulators) are classified by Z_2 topological invariants [5] which take two values, 1 or 0, thereby providing a distinction between topological and normal insulators. Mathematically, one can construct Z_2 invariants in different ways, but their physical meaning always relies on the symmetry of electron wave function which is changed as a result of energy band inversion. Such an inversion occurs due to spin-orbit coupling and Darwin term contributions in the Hamiltonians of the crystals formed from heavy atoms. There are three types of band inversions ($s - p$, $p - p$, and $d - f$) in the three-dimensional (3D) TI discovered so far [6].

The most extensively studied TI materials, bismuth chalcogenides and related alloys, belong to $p - p$ inversion type. For thin layers of these materials, one expects a dimensionality crossover: when layer thickness d decreases, the material transforms from 3D TI into two-dimensional (2D) TI [7]. This occurs when the wave function decay length of the surface states becomes comparable to d . As a result, the 2D states from opposite surfaces hybridize and their spectrum is no longer gapless [7, 8]. On the other hand, since the surface states in TI cover the whole surface of the layer, including side regions, they are transformed into 1D conducting edge channels in these regions, Fig. 1 (a), [9].

A special place in this connection belongs to HgTe, a zinc-blend-structure crystal with $s - p$ band inversion, where the energy of p -type Γ_8 band in the Γ point of Brillouin zone is higher than the energy of s -type Γ_6 band. In spite of the inversion, bulk HgTe is not a 3D TI because it is a symmetry-protected gapless material. A gap can be opened in a thin HgTe layer sandwiched between $\text{Cd}_{1-x}\text{Hg}_x\text{Te}$ layers (normal insulators), as realized in epitaxially grown quantum wells (QWs). Due

to size quantization, the heavy hole (hh) continuum that forms the valence band in HgTe splits into a set of 2D states hybridized with two interface-like states $S1$ and $S2$, Fig. 1 (b). The gap between the ground-state hh subband ($hh1$) and the next adjacent subband exists for QW narrower than 18 nm (for wider wells the QW is in a semimetallic state). Since the gap opening is accompanied with the dimensionality crossover, a HgTe-based QW should be a 2D TI having edge states in the gap between subbands. However, a direct theoretical proof for this statement, based on a two-subband effective 2D Hamiltonian [10], has been done only for a special situation when $S1$ subband is just slightly below $hh1$ subband, which is applicable to narrow wells in the width range of approximately 6.3 – 8.3 nm. The edge state transport in such QWs was also confirmed experimentally [11]. In wider HgTe QWs, any effective Hamiltonian methods are not generally feasible because of a complicated subband structure, though a usage of three-subband ($S1$, $hh1$, and $hh2$) basis [12] extends the range of applicability of such methods. In particular, it was found that when $S1$ subband falls below $hh2$ one (so the principal gap is formed between $hh1$ and $hh2$ subbands) the edge states exist both in this gap and in the next gap between $hh2$ and $S1$ subbands.

A question that naturally arises concerns persistence of 2D TI state in wide QWs where the $S1$ subband lies below several hh subbands, so the situation is far different from that described theoretically in Refs. [10] and [12]. From the point of view of dimensionality crossover, there are no reasons to deny the 2D TI nature of these systems, since widening of the QW (actually, approaching of HgTe layer to the bulk state) does not cancel the fact of $s - p$ inversion in this layer and, accordingly, cannot destroy the edge states. In this Letter we report experimental investigation of 14 nm wide HgTe QWs which are wider than those studied previously [11, 13, 14] but still have a sizeable gap of a few meV between $hh1$ and $hh2$ subbands. We plot the expected edge states in this gap schematically in Fig. 1 (c) as two (one for each spin number) gapless branches merging with 2D subbands on a tangent. By transport measurements, we indeed ob-

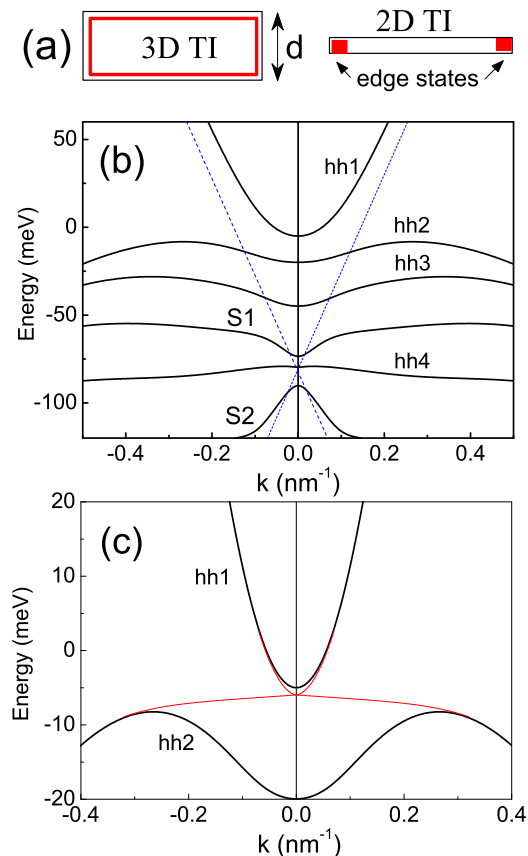


FIG. 1: (Color online) (a) Cross-section of a 3D TI sample (schematic) with surface state channels shown in red. As the thickness of the sample decreases, a transition to 2D TI takes place. (b) Energy spectrum of size-quantized subbands in a symmetric 14 nm wide Cd_{0.65}Hg_{0.35}Te/HgTe/Cd_{0.65}Hg_{0.35}Te QW, calculated numerically by using Kane Hamiltonian. Dashed (blue) lines show the spectrum of interface states at a single HgTe/Cd_{0.65}Hg_{0.35}Te boundary under approximation that mixing of these states with hh states is neglected. (c) A magnified picture of two upper hh subbands and expected edge state spectrum, thin (red) lines, in the gap between them.

tain numerous proofs for the edge state transport in these QWs.

The experimental samples are Hall bridges fabricated on top of the 14 nm wide HgTe QW with the surface orientation (112) and provided with electrostatic gate. Their fabrication technology is described in detail in [15]. Three different types of experimental samples were used: macroscopic Hall bridges (see Fig. 2) with the width 50 μm and the distance between the voltage probes 100 μm and 250 μm , and two types of microscopic samples, whose layout together with the scale is shown in Fig. 3 [16]. The transport measurements were conducted in the temperature range 0.2 – 10 K and in magnetic fields up to 10 T using the standard phase detecting scheme or

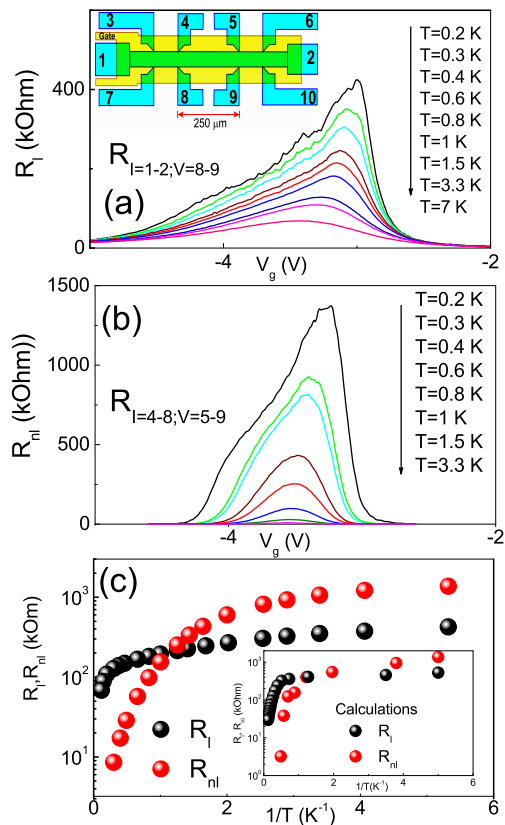


FIG. 2: (Color online) Local (a) and nonlocal (b) resistance at different temperatures, sample I, $B = 0$ (insert - schematic view of the sample). (c) Temperature dependence of local and nonlocal resistance when the Fermi energy is situated in the center of the insulating bulk gap (insert - calculation).

frequencies 3 – 12 Hz and the driving current 0.1 – 1 nA to avoid heating effects. The electron mobility μ in all samples studied was above 10^5 $\text{cm}^2/\text{V s}$ for the carrier density 3×10^{11} cm^{-2} .

We first consider the properties of our macroscopic samples. Observation of both local (R_l) and nonlocal (R_{nl}) resistance in the absence of magnetic field is generally considered as a direct proof of 2D TI state. In that case the current flows through a sample along its borders and resistance exists regardless to positions of voltage probes with respect to current contacts, either in ballistic [13] or diffusive [14] regime. Figures 2 (a) and 2 (b) show R_l and R_{nl} as functions of the gate voltage for various temperatures in the range 0.2–3.3 K and Fig. 2 (c) shows these resistances as functions of temperature for the gate voltages corresponding to the maxima of local and nonlocal resistance, i.e. when the Fermi level is in the middle of the insulating gap. Qualitatively, the behavior of local and nonlocal resistances is similar. When the temperature is above 1 K, both resistances grow exponentially with decreasing temperature. For lower temperatures the resistance growth slows down and for $T < 0.5$ K it obeys a power law $R \propto T^{-\alpha}$ ($\alpha \approx 0.5$). As this takes place,

even though at higher temperatures the local resistance is several orders of magnitude greater than the nonlocal one, at $T < 1$ K the nonlocal resistance becomes larger. The described behavior of R_l and R_{nl} is typical for the 2D TI, as it follows from the fundamental difference in the relative contributions of the bulk and edge transport when measuring in local and nonlocal configurations [14]. At higher temperatures, when the bulk contribution is still sufficiently large, R_{nl} is exponentially small compared to the sheet resistivity. With decreasing T the bulk contribution to transport also decreases, and at some T , depending on the insulating bulk gap, becomes negligibly small. Under these conditions the difference in the resistance values measured in local and nonlocal configurations is determined only by the distribution of currents flowing along the sample perimeter and by the position of the voltage probes. At $T < 0.5$ K for all investigated configurations the resistance at its maximum is more than an order of magnitude greater than $h/2e^2$ which means that the transport via the edge states is diffusive.

Let us discuss in more detail the temperature dependence of R_{nl} and R_l . First, the maximum of the curves $R_{nl}(V_g)$ and $R_l(V_g)$ shifts to the right with the temperature decreasing. Such behavior was not observed in 2D TI previously and is probably related to the complicated energy spectrum of the system investigated, or, more specifically to its much smaller gap which is further diminished by the bulk bands density of states tails. Second, as has already been mentioned, with lowering temperature the resistance, after the exponential growth, continues to increase, but at a much lower rate, following a power law $R \propto T^{0.5}$, typical for quasi 1D wires in a weak localization regime. We have attempted a quantitative description of the temperature dependence of the local and nonlocal resistance peak values by using the model proposed in [16, 17]. The activation energy for the bulk transport has been chosen as a fitting parameter. The results of the calculation presented in Fig. 2 (c) show a reasonable agreement between the calculated and measured dependences. The value of the activation energy found from fitting the calculation to experiment is approximately 1.2 meV for local and nonlocal configurations alike, as was expected. This value is less than $\Delta = 3.3$ meV, the indirect insulating gap value obtained from the energy spectrum calculation. This discrepancy is not surprising if one considers the disorder due to impurities and QW thickness fluctuations that is always present in a real HgTe sample. In such case one may expect that the activation energy would correspond to the mobility gap rather than to a much larger calculated insulating bulk gap [18].

The mean free path for the edge states transport determined experimentally for the diffusive transport in the macroscopic samples is $2 - 5 \mu\text{m}$ for sample I and $12 - 14 \mu\text{m}$ for sample II (See supplementary material). On this account our QWs look promising for observation of ballistic transport via edge states, considering that in the majority of the previously studied 2D TI this value was

close to $1 \mu\text{m}$. For this purpose, two types of microscopic samples were fabricated, one with the dimensions $W = 1.7 \mu\text{m}$ and $L = 1.8 \mu\text{m}$ (see Insert to Fig.3a) and the other an H-shaped bridge with the width $W = 3.2 \mu\text{m}$ and the length $L = 2.8 \mu\text{m}$ (see Insert to Fig.3b).

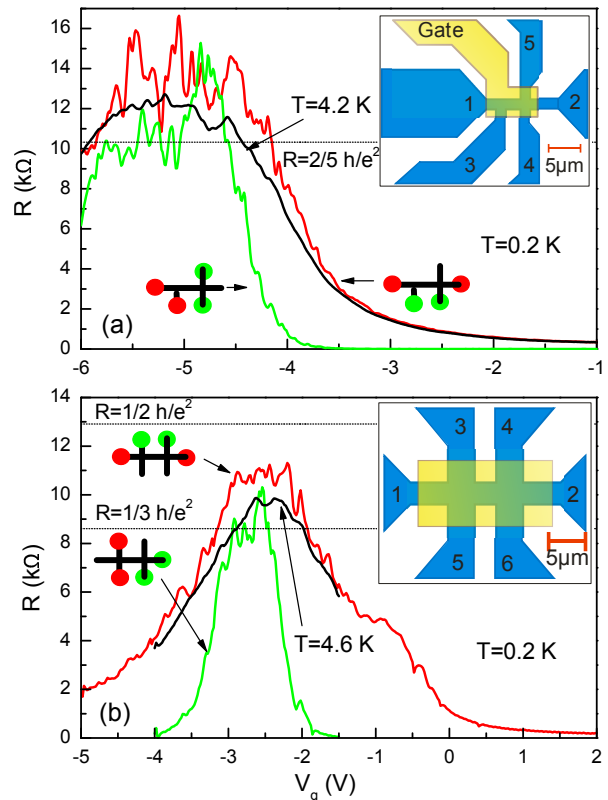


FIG. 3: (Color online) $R(V_g)$ dependences for local (red curves) and nonlocal (green curves) resistance measurement configurations obtained in two different types of microscopic samples. The samples layouts are shown schematically in the Inserts. All curves were obtained at 0.2 K except the black curves measured at temperatures 4.2 and 4.6 K. Opposite each curve the corresponding measurement configuration is shown schematically. The dashed horizontal lines mark the resistance values expected for these configurations in the case of a purely ballistic transport via edge current states.

Figure 3 shows the dependence of the local (red color) and nonlocal (green color) resistance versus gate voltage measured in the two microscopic samples. When the bias applied to the gate decreases below -1 V (Fig.3a) (2 V in Fig.3b), the local resistance starts to grow gradually as the Fermi level first descends to the bottom of the conduction band and then enters the insulating bulk gap at $V_g \approx -4.5$ V (Fig.3a) ($V_g \approx -2$ V in Fig.3b). The nonlocal response is close to zero when the Fermi level remains in the conduction band. The abrupt increase in the nonlocal resistance as the Fermi level enters the insulating gap signals, as well as in the macroscopic case, the presence of the edge current states in the gap. The calculation of the local and nonlocal resistance values expected in our microstructures in the case of ballistic transport

via edge states is quite simple and is indicated by the dashed lines for each configuration shown in Fig.3. As may be seen, the average resistance values measured at $T = 0.2$ K in the gate voltage range corresponding to the Fermi level staying in the insulating gap are quite close to the levels expected for purely ballistic transport. With the negative bias increasing the Fermi level enters the valence band and the sample resistance decreases. Relying on this data, it is possible to conclude that our microstructures demonstrate a quasiballistic edge transport in a 2D TI. This fact is quite important considering that up till now the observations of ballistic transport in HgTe-based 2D TI reported in [11] has remained unique. We also observe other similarities with the results reported in [11]. In particular, when the Fermi level lies in the insulating gap there are random fluctuations both in the local and nonlocal resistance. The amplitude of these fluctuations sharply decreases as the temperature increases indicating their mesoscopic origin.

Figure 3 also shows the variation of the local resistance with temperature in the range from 0.2 K to 4.2K in our microstructures. One can see that this variation is noticeably weaker than in our macroscopic samples (compare with Fig. 2 (c)). This fact has a simple explanation. In microstructures the sheet conductance due to the bulk transport is the same as in macroscopic samples while the resistance to transport via edge states decreases by approximately one order of magnitude. This observa-

tion also indicates that the mean free path for the edge states transport in our QWs must be comparable to or higher than $\approx 10 \mu\text{m}$. We also observe a suppression of both local and nonlocal quasiballistic conductance by weak magnetic field, a behavior typical for 2D TI state [11, 19], which will be reported elsewhere.

We believe that our observation of relatively high mean free path for the edge states is not accidental but rather related to the advantages associated with the use of a wider quantum well. Indeed, the width of any QW is not uniform but fluctuates from point to point around its average value d with the amplitude δ . That δ is determined by the growth technology employed and is practically independent of the QW width. The fluctuation of the QW width results in a random potential in the bulk of the QW. However, the amplitude of that random potential would be much smaller in a wider QW as it is proportional to $1/(d^3)$. From that point of view it is clear that a wider QW well is more advantageous for the observation of ballistic transport in 2D TI.

The results of the present study confirm that the 2D TI state in HgTe QWs is quite robust and exists in a sizeable range of well widths despite of the fact that the energy spectrum in such QWs is complicated and strongly dependent on the well width.

The work was supported by the RFBI grants, by the RAS grant 24.11 and by FAPESP, CNPq (Brazilian agencies).

-
- [1] M. Z. Hasan and C. L. Kane, Rev. Mod. Phys. **82**, 2045 (2010); X-L. Qi, S-C. Zhang, Rev. Mod. Phys. **83**, 1057 (2011).
- [2] X-L. Qi, S-C. Zhang, Phys. Today **63(1)**, 33 (2010).
- [3] J. E. Moore and L. Balents, Phys. Rev. B **75** 121306 (2007).
- [4] J. E. Moore, Nature (London) **464**, 194 (2010).
- [5] C. L. Kane and E. J. Mele, Phys. Rev. Lett. **95**, 146802 (2005).
- [6] H. Zhang, S-C. Zhang, Phys. Status Solidi RRL **7**, 72 (2013).
- [7] C.-X. Liu, H.Zhang, B. Yan, X.-L. Qi, T. Frauenheim, X. Dai, Z. Fang, S.-C. Zhang, Phys. Rev. B **81**, 041307 (2010).
- [8] H.-Z. Lu, W.-Yu. Shan, W. Yao, Q. Niu, and S.-Q. Shen, Physical Review B **81**, 115407 (2010).
- [9] L. Wu, M. Brahlek, R. V. Aguilar, A. V. Stier, C. M. Morris, Y. Lubashevsky, L. S. Bilbro, N. Bansal, S. Oh, and N. P. Armitage, Nature Physics **9**, 410 (2013).
- [10] B. A. Bernevig, T. L. Hughes, and S. C. Zhang, Science **314**, 1757 (2006).
- [11] M. König, S. Wiedmann, C. Brune, A. Roth, H. Buhmann, L. W. Molenkamp, X.-L. Qi, and S.-C. Zhang, Science **318**, 766 (2007).
- [12] O. E. Raichev, Phys. Rev. B **85**, 045310 (2012).
- [13] A. Roth, C. Brüne, H. Buhmann, L. W. Molenkamp, J. Maciejko, X.-L. Qi, and S.-C. Zhang, Science **325**, 294 (2009).
- [14] G. M. Gusev, Z. D. Kvon, O. A. Shegai, N. N. Mikhailov, S. A. Dvoretzky and J. C. Portal, Phys. Rev. B **84**, 121302(R) (2011).
- [15] Z. D. Kvon, E. B. Olshanetsky, D. A. Kozlov, E. G. Novik, N. N. Mikhailov, and S. A. Dvoretzky, Low Temperature Physics **37**, 202 (2011).
- [16] See Supplemental Material for details on the sample description, bulk+edge model, and magnetoresistance measurements.
- [17] G. M. Gusev, E. B. Olshanetsky, Z. D. Kvon, A. D. Levin, N. N. Mikhailov, and S. A. Dvoretzky, Phys. Rev. Lett. **108**, 226804 (2013).
- [18] R. E. Prange, S. M. Girvin (Eds) *The Quantum Hall Effect* (New York, Springer-Verlag, 1987)
- [19] G. M. Gusev, E. B. Olshanetsky, Z. D. Kvon, N. N. Mikhailov and S. A. Dvoretzky, Phys. Rev. B, **87**, 081311 (R) (2013).

Online supplemental material to : Persistence of two-dimensional topological insulator state in wide HgTe quantum well

E. B. Olshanetsky,¹ Z. D. Kvon,^{1,2} G. M. Gusev,³ A. D. Levin,³

O. E. Raichev,⁴ N. N. Mikhailov,¹ and S. A. Dvoretzky,¹

¹*Institute of Semiconductor Physics, Novosibirsk 630090, Russia*

²*Novosibirsk State University, Novosibirsk 630090, Russia*

³*Instituto de Física da Universidade de São Paulo, 135960-170, São Paulo, SP, Brazil and*

⁴*Institute of Semiconductor Physics, NAS of Ukraine, Prospekt Nauki 41, 03028 Kyiv, Ukraine*

(Dated: August 23, 2018)

In this supplementary, we provide details on the sample description, the mean free path calculation and the model taking into account the edge and bulk contribution to the total current.

SAMPLE DESCRIPTION

In the main text we describe the experimental results in macroscopic and mesoscopic samples in zero magnetic field. The $\text{Cd}_{0.65}\text{Hg}_{0.35}\text{Te}/\text{HgTe}/\text{Cd}_{0.65}\text{Hg}_{0.35}\text{Te}$ quantum wells with surface orientation (112) studied here were grown by molecular beam epitaxy (MBE). The schematic view of the samples layer structure is shown in Fig. 1a. As shown in previous publications [1], the use of substrates inclined to the singular orientations may lead to the growth of more perfect films. Therefore, the efficient growth of alloys is done predominantly on substrates with surface orientations of (112), which deviate from the singular planes by approximately 19° . We have investigated samples of both macroscopic and microscopic dimensions. The microscopic devices were of two types. The first with the dimensions $W = 1.73 \mu\text{m}$ and $L = 1.8 \mu\text{m}$ and the other an H-type bridge with the width $W = 3.2 \mu\text{m}$ and the length $L = 2.8 \mu\text{m}$, Fig. 1 (b). The macroscopic sample consists of 3 narrow ($50 \mu\text{m}$ wide) consecutive segments of different length (100, 250, $100 \mu\text{m}$), and 8 voltage probes, Fig.1(c). The ohmic contacts to the two-dimensional gas were formed by the in-burning of indium. To prepare the gate, a dielectric layer containing 100 nm SiO_2 and 100 nm Si_3Ni_4 was first grown on the structure using the plasmochemical method. Then, the TiAu gate was deposited.

Low-temperature magnetotransport measurements were carried out to identify the charge neutrality point (CNP) and to obtain the relation between the induced carrier density and the gate voltage V_g . Sweeping the gate voltage, we have found a continuous crossover from electron to hole type of conductivity, when the Fermi level is shifted from the conduction to the valence band. The possibility to tune the carrier density electrostatically enables the observation of electron and hole transport in a single device, making it possible to control the filling of Landau levels in the presence of the perpendicular magnetic field. Figure 2 shows longitudinal ρ_{xx} and Hall ρ_{xy} resistivities as functions of the gate voltage at a fixed magnetic field $B = 2 \text{ T}$. Pronounced plateaus with values $\rho_{xy} = h/\nu e^2$ are clearly seen for electrons at

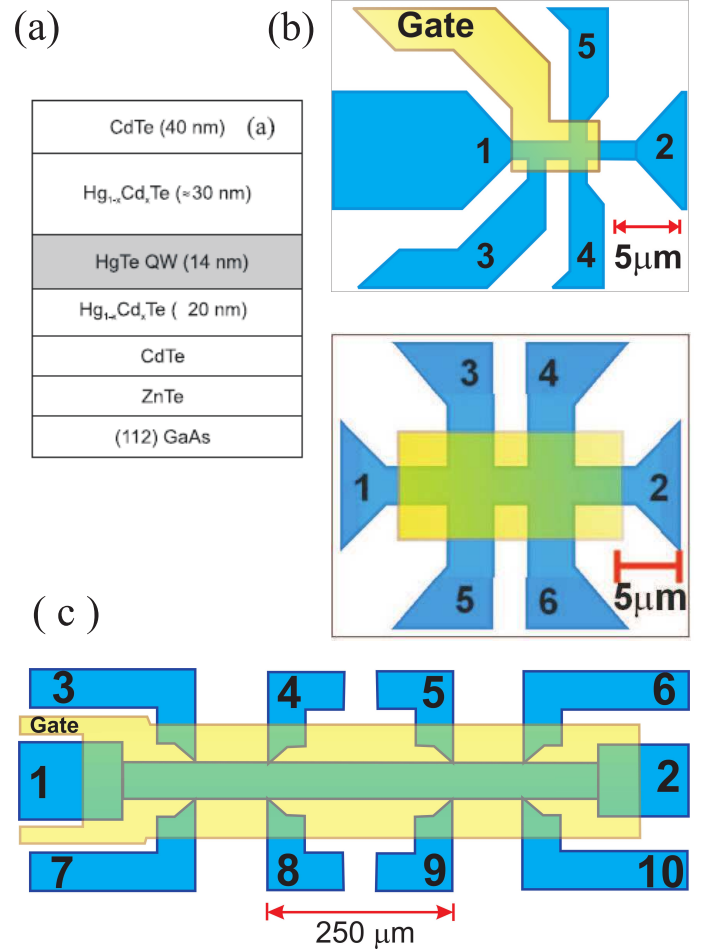


FIG. 1: (Color online) (a) Schematic layer structure of a wafer containing 14 nm HgTe QW. (b) mesoscopic samples topology, yellow rectangular area depicts the gate; (c) macroscopic samples layout.

ν from -1 to -5 , accompanied by deep minima in R_{xx} . As V_g is swept through the CNP, when the Fermi level is in the middle of the gap, the longitudinal resistivity shows a maximum, whereas ρ_{xy} goes gradually through zero from negative on the electron side to positive on the hole side. It is a clear indication of CNP position and

electron-hole crossover as a function of the gate voltage. Observation of the edge state transport near CNP in zero magnetic field is described in the main text. From the resistance minima we obtain the density variation with gate voltage $8.4 \times 10^{14} \text{ m}^{-2} \text{ V}^{-1}$, which coincides with the density extracted from the capacitance.

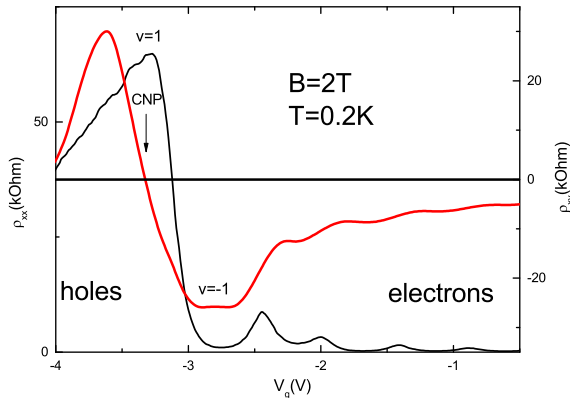


FIG. 2: (Color online) (a) Longitudinal ρ_{xx} (black line) and Hall ρ_{xy} (red line) resistivities as functions of the gate voltage at a fixed magnetic field, $B = 2.0 \text{ T}$. Vertical arrow indicates CNP.

MEAN FREE PATH CALCULATION FOR THE EDGE STATES TRANSPORT

At $T < 0.5 \text{ K}$ for all investigated measurement configurations in the macroscopic sample the resistance at its maximum is more than an order of magnitude greater than $h/2e^2$ which means that the transport via the edge states is diffusive. In this case there is a simple expression that allows one to calculate the resistance value for any measurement configuration assuming that there is only edge state transport in the sample: $R_{n,m}^{i,j} = \frac{L_{n,m} L_{i,j}}{lL} (h/e^2)$, where $R_{n,m}^{i,j}$ is the resistance measured between contacts i and j while the current is maintained between contacts n and m , $L_{i,j}$ ($L_{n,m}$) are the distances between i and j (n and m) along the sample edge that does not include n and m (i and j), L is the total perimeter of the sample, and l is the mean free path. Thus, it is possible to determine the mean free path l for the transport via the edge states. Table 1 presents the results obtained in this way for samples I and II. The values of l derived from different measurement configurations in the same sample are quite close, but may differ substantially in different samples. This data supports the statement advanced in [2] that in 2D TI fabricated on the basis of HgTe QWs with inverted energy spectrum the edge states have a macroscopic length (about a millimeter).

Sample	Config.	l (μm)
I	R_{1-2}^{8-9}	4.6
I	R_{4-8}^{5-9}	3.6
I	R_{1-2}^{7-8}	2.6
II	R_{1-2}^{3-4}	12
II	R_{1-2}^{7-8}	12
II	R_{1-2}^{8-9}	14
II	R_{5-9}^{4-8}	13
II	R_{3-7}^{4-8}	12.5
II	R_{3-7}^{5-9}	11.6

TABLE I: The first column: sample number. The second column: various local and nonlocal measurement configurations. The third column: mean free path for the edge states transport obtained from the comparison of the peak resistance value with theory.

On the other hand, it is in agreement with a conclusion made earlier [2, 3] concerning the absence of topological protection against backscattering on the scale of few microns and longer.

EDGE+BULK MODEL

In the main text it has been demonstrated that the resistance of HgTe quantum wells reveals a broad peak when the gate voltage induces an additional charge density altering the quantum wells from n-type conductor to p-type one around the charge neutrality point (CNP). The peak amplitude is approximately equal to $h/2e^2$ in mesoscopic samples, due to nearly ballistic edge-state transport, and $R \gg h/2e^2$ in macroscopic samples. The lack of the robustness of resistance quantization against intrinsic and introduced disorder in macroscopic samples may be explained in various ways [4–6]. Independently of the particular microscopic mechanism responsible for this, the resistance can be described by the combination of the edge-state and bulk transport contributions, with taking into account both the backscattering within one edge and bulk-edge coupling. The local and nonlocal transport coefficients arise from the edge state contribution and short-circuiting of the edge transport by the bulk contribution, the latter is more important away from the CNP. Below we reproduce the basic features of this model [7, 8]. The transport properties in the bulk can be described by the current-potential relation

$$\mathbf{j}_i(\mathbf{r}) = -\hat{\sigma}_i \nabla \psi_i(\mathbf{r}), \quad (1)$$

$$\hat{\sigma}_i = \begin{pmatrix} \sigma_{xx}^{(i)} & \sigma_{xy}^{(i)} \\ \sigma_{yx}^{(i)} & \sigma_{xx}^{(i)} \end{pmatrix},$$

where $i = 1, 2$ numbers the states with different projections of the spin, ψ_i are the electrochemical potential for

electrons, and $\mathbf{r} = (x, y)$ is the 2D coordinate. As we consider the isotropic conduction, the non-diagonal part of the conductivity tensor appears only at non-zero magnetic field. Assuming the components of the conductivity tensor as coordinate-independent parameters, we can solve the problem by solving the Laplace equation for the potentials, $\nabla^2 \psi_i(\mathbf{r}) = 0$, because the charge conservation continuity conditions requires $\nabla \mathbf{j}_i(\mathbf{r}) = 0$. A solution to Laplace equation is uniquely determined by specifying boundary conditions, which in our case are modified by the bulk-edge current leakage. In order to describe the transport in the presence of the edge states, we introduce two phenomenological constants γ and g , which represent edge to edge and bulk to edge inverse scattering length, respectively. Then, the boundary conditions expressing zero current normal to the boundary in the presence of the bulk-edge coupling are given by

$$\mathbf{n} \mathbf{j}_i = g(\psi_i - \varphi_i), \quad (2)$$

where φ_i are the local chemical potentials of the edge states, ψ_i and \mathbf{j}_i are the potentials and currents at the boundary, and \mathbf{n} is a unit vector normal to the boundary.

The edge state transport can be described by continuity equations [7, 9] taking into account the scattering between edge and bulk:

$$\partial_x \varphi_1 = \gamma(\varphi_2 - \varphi_1) + g(\psi_1 - \varphi_1), \quad (3)$$

$$-\partial_x \varphi_2 = \gamma(\varphi_1 - \varphi_2) + g(\psi_2 - \varphi_2). \quad (4)$$

The general solution of this problem, therefore, includes solution of a 2D Laplace equation for the bulk electrochemical potentials $\psi_{1,2}(x, y)$ together with Eqs. (2),(3),(4) describing the scattering between edge states and between edge and bulk states. The current can be calculated from this solution as a sum of the contributions from bulk and edge states.

In nonlocal configurations the edge + bulk model can be solved only numerically. We have performed self-consistent calculations to find $\psi_{1,2}$ solution of Laplace equation in two space dimensions and $\varphi_{1,2}$ solutions of equations 3 and 4 on the edge using the Hall bar geometry schematically shown in Fig. 1 (c) [or Fig. 2 of the main text]. The contacts are assumed to be thermal reservoirs, where full mixing of electron spin states and bulk states occurs [9]. Note that, in contrast to the standard QHE, when mixing of the edge states occurs within metallic Ohmic contacts, in our samples potential mixing is provided by 2D electron gas in the region outside of the metallic gate.

The equations for $\psi_{1,2}$ are discretized by the finite element method. The generalized Neumann boundary conditions, Eq. (2), are set in the regions outside the metal contacts. To solve the boundary value problem for a system of ordinary differential equations (3) and (4) we use a finite difference code that implements the 3-stage Lobbato IIIa formula. The boundary conditions inside the metal contacts are set to $\varphi_{1,2} = \psi_{1,2}$.

For both local and non-local configurations, the resistance is calculated as

$$R_{xx} = V I_{tot}^{-1}, \quad I_{tot} = I_{edge} + I_{bulk},$$

$$V = \frac{1}{2} (\varphi_{11} - \varphi_{11'} + \varphi_{21} - \varphi_{21'}), \quad (5)$$

where V is the potential difference at the voltage probes, I_{tot} is the total current flowing between current contacts, φ_{i1} and $\varphi_{i1'}$ are the potentials at the voltage probe locations. The edge and bulk currents for the local case (at arbitrary point x along the sample) are given by

$$I_{edge} = \frac{e^2}{h} (\varphi_1 - \varphi_2 + \varphi_{2'} - \varphi_{1'}),$$

$$I_{bulk} = \sum_{i=1,2} \left[\sigma_{xy}^{(i)} (\psi_i - \psi_{i'}) - \sigma_{xx}^{(i)} \int dy \frac{\partial \psi_i}{\partial x} \right], \quad (6)$$

where φ_i , ψ_i and $\varphi_{i'}$, $\psi_{i'}$ are the potentials at the opposite (bottom and top, respectively) edges of the sample, and the integral is taken across the sample from bottom to top. For non-local case the currents are calculated from similar expressions:

$$I_{edge} = \frac{e^2}{h} (\varphi_1 - \varphi_2 + \varphi_{2'} - \varphi_{1'}),$$

$$I_{bulk} = \sum_{i=1,2} \left[\sigma_{yx}^{(i)} (\psi_i - \psi_{i'}) - \sigma_{xx}^{(i)} \int dx \frac{\partial \psi_i}{\partial y} \right], \quad (7)$$

where now φ_i , ψ_i and $\varphi_{i'}$, $\psi_{i'}$ are the potentials at the opposite (left and right, respectively) edges of the current contact, and the integral is taken across this current contact from left to right.

The conductivities are calculated as $\sigma_{xx}^{(1)} = \sigma_{xx}^{(2)} = e(\mu_n n + \mu_p p)/2$, where μ_n and n (μ_p and p) are electron (hole) mobilities and densities. To find n and p , the bulk densities of states for electrons and holes are represented by steps $D_{n,p} = 4\pi m_{n,p}/h^2$ with $m_{n,p}$ being the effective masses of electrons and holes. The energy gap separating electron and hole bands is $E_g = 3.3$ meV. In addition, the sharp band edges are smoothed according to a Gaussian law with broadening energies $\Gamma_{n,p} = \hbar/\tau_{n,p}$, where $\tau_{n,p} = \mu_{n,p} m_{n,p}/e$. The following parameters have been used: $\mu_n = 80000$ cm²/V s, $\mu_p = 5000$ cm²/V s, $m_n = 0.024 m_0$, $m_p = 0.15 m_0$, where m_0 is the free electron mass. The extended states are separated by a mobility gap ~ 1 meV. Our calculations reproduce the temperature dependence of the local and nonlocal resistances, shown in Fig. 2 of the main text. The best agreement between the experiment and theory is reached for parameters $\gamma^{-1} = g^{-1} = 5$ μ m, which roughly agrees with the mean free path l represented in the Table I of the main text. Parameters γ and g are assumed to be independent of temperature.

-
- [1] Z. D. Kvon, E. B. Olshanetsky, E. G. Novik, D. A. Kozlov, N. N. Mikhailov, I. O. Parm, and S. A. Dvoretzky, *Phys. Rev. B* **83**, 193304 (2011).
- [2] G. M. Gusev, Z. D. Kvon, O. A. Shegai, N. N. Mikhailov, S. A. Dvoretzky and J. C. Portal, *Phys. Rev. B* **84**, 121302(R) (2011).
- [3] M. König, S. Wiedmann, C. Brune, A. Roth, H. Buhmann, L. W. Molenkamp, X.-L. Qi, and S.-C. Zhang, *Science* **318**, 766 (2007).
- [4] J. Maciejko, C. X. Liu, Y. Oreg, X. L. Qi, C. Wu, and S. C. Zhang, *Phys. Rev. Lett.* **102**, 256803 (2009).
- [5] A. Ström, H. Johannesson, and G. I. Japaridze, *Phys. Rev. Lett.* **104**, 256804 (2010).
- [6] J. I. Vayrynen, M. Goldstein, and L. I. Glazman, *Phys. Rev. Lett.* **110**, 216402 (2013).
- [7] D. A. Abanin, K. S. Novoselov, U. Zeitler, P. A. Lee, A. K. Geim, and L. S. Levitov, *Phys. Rev. Lett.* **98**, 196806 (2007).
- [8] G. M. Gusev, E. B. Olshanetsky, Z. D. Kvon, A. D. Levin, N. N. Mikhailov, and S. A. Dvoretzky, *Phys. Rev. Lett.* **108**, 226804, (2012).
- [9] V. T. Dolgoplov, G. V. Kravchenko, and A. A. Shashkin, *Sol. St. Commun.* **78**, 999 (1991).